Journal of
Materials Chemistry A

Accepted Manuscript

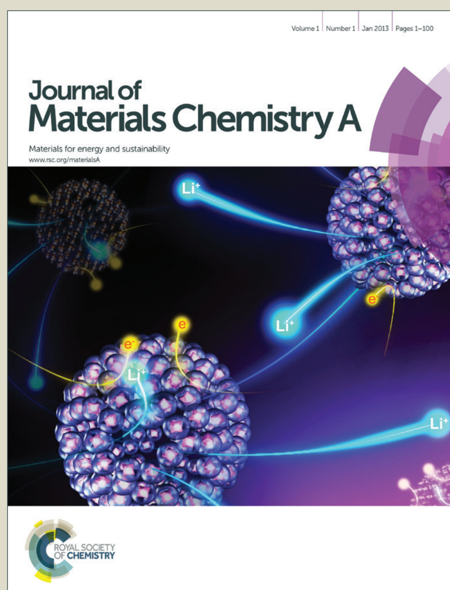

This is an *Accepted Manuscript*, which has been through the Royal Society of Chemistry peer review process and has been accepted for publication.

Accepted Manuscripts are published online shortly after acceptance, before technical editing, formatting and proof reading. Using this free service, authors can make their results available to the community, in citable form, before we publish the edited article. We will replace this *Accepted Manuscript* with the edited and formatted *Advance Article* as soon as it is available.

You can find more information about *Accepted Manuscripts* in the Information for Authors.

Please note that technical editing may introduce minor changes to the text and/or graphics, which may alter content. The journal's standard Terms & Conditions and the Ethical guidelines still apply. In no event shall the Royal Society of Chemistry be held responsible for any errors or omissions in this *Accepted Manuscript* or any consequences arising from the use of any information it contains.

ROYAL SOCIETY OF CHEMISTRY

www.rsc.org/materialsA

Highly active ruthenium oxide coating via ALD and electrochemical activation in supercapacitor applications

Roseanne Warren,[1] Firas Sammoura,[1,2] Fares Tounsi,[1] Mohan Sanghadasa[3] and Liwei Lin[1,*]

[1]Berkeley Sensor & Actuator Center, 403 Cory Hall #1774, University of California, Berkeley, CA 94720-1774, USA

[2]Department of Electrical Engineering and Computer Science, Masdar Institute of Science and Technology, Abu Dhabi, UAE

[3]Aviation and Missile Research, Development, and Engineering Center, USA

*lwlin@berkeley.edu

Abstract

Highly active ruthenium oxide was uniformly coated on vertically aligned carbon nanotube forests for pseudocapacitor electrodes in enhanced energy storage applications. Atomic layer deposition (ALD) was designed to realize the conformal coating process onto porous structures and an electrochemical oxidation process was developed to achieve highly active ruthenium oxide. Results show 100x and 170x higher specific capacitance after the ALD coating and further electrochemical oxidation process, respectively, as compared with that of pure CNT electrodes. Furthermore, the measured capacitance value was close to the theoretical limit of ruthenium oxide at 644 F/g with a high power density at 17 kW/kg. The electrode performance was tested over 10,000 charge-discharge cycles with gradually improved capacitance of 17% higher than the starting value and at ultra-high scan rates of up to 20 V/s.

Keywords

Energy storage, pseudocapacitors, atomic layer deposition, metal oxides, carbon nanotubes

Journal of Materials Chemistry A Accepted Manuscript

Introduction

Supercapacitors store charge in the form of electric double layer capacitance or by additional surface or near-surface Faradiac reactions by means of pseudocapacitance.[1,2] Large surface area electrodes and highly active pseudocapacitive materials are paramount for achieving high performance supercapacitors.[3–5] Ruthenium oxide (RuO_x) is well-known as one of the highest performing pseudocapacitive materials,[6,7] among other candidates including manganese oxide (MnO_2),[8–12] vanadium oxide (V_2O_5),[13] and mixed cobalt-nickel oxides (a-$(Co+Ni)(OH)_2 \cdot nH_2O$).[14] These metal oxide pseudocapacitive materials require good proton and electron conductivity for high performance, as positive ions (H^+) are intercalated during the charging process.[15] As a result, hydrated amorphous oxides display higher charge storage capability due to better proton conductivity and more electrochemically active redox sites.[16]

To achieve high specific capacitance, RuO_x fabrication methods must provide excellent control of electrode structure and chemical composition as well as good uniformity over high surface areas. RuO_x-porous carbon composite electrodes have been constructed to increase surface area, provide high double layer capacitance, and reduce electrode material cost.[17] Previous fabrication methods of RuO_x supercapacitors include solution-based deposition from ruthenium trichloride ($RuCl_3$)[18–21] and ruthenium nitrosyl nitrate,[22] however these methods often result in poor uniformity of the RuO_x coating. Other fabrication methods include magnetic sputtering,[23] electro-oxidation of Ru nanoparticles,[24] and mixing of RuO_2-xH_2O particles with a polymer binding agent.[25] These approaches yield poor electron conductivity, low utilization of RuO_x due to non-uniformly dispersed nanoparticles or films, and low proton conductivity due to poor hydration in the case of non-solution methods.

Atomic layer deposition (ALD) is a high-precision chemical vapor deposition technique that uses sequential pulsing of precursors to deposit nanoscale films monolayer by monolayer. With ALD, conformal and uniform films of metal, oxide, and nitride materials can be deposited onto high surface area substrates.[26] Recently, there has been growing interest in ALD for catalysis, sensing, and energy conversion, as well as DRAM and CMOS commercial technologies.[27] To date, there have been only two investigations of ALD for supercapacitor applications: vanadium oxide (VO_x)[28] and titanium dioxide (TiO_2) supercapacitors.[29] Although these works demonstrated conformal coating of the pseudocapacitive material, there has yet to be an investigation of optimal ALD material chemistry for maximum proton conductivity and pseudocapacitor performance.

In this work, we provide important insight into the nature of hydration of ALD metal oxide films, and devise the use of post-ALD electrochemical oxidation to achieve high specific capacitance for ALD pseudocapacitors, using RuO_x as a demonstration material. ALD RuO_x poses unique challenges for supercapacitor applications as: 1) the degree of oxidation is difficult to control, with reports ranging from pure metallic Ru to pure RuO_2 films,[30–32] and 2) the ALD process in vacuum and at elevated temperatures (270 °C-400 °C) is not conducive to depositing a hydrated oxide. Specific accomplishments of this work include: uniform, conformal coating of high-surface area porous electrodes with RuO_x; rapid charge/discharge response due to direct bonding of the RuO_x coating to the electrode, with high durability for flexible electrodes; and achieving pseudocapacitance values on-par with the highest values reported in the literature for RuO_x.[1,3] In this work, ALD RuO_x films are deposited on vertically aligned

Journal of Materials Chemistry A Accepted Manuscript

carbon nanotube (CNT) forests and porous silicon (Si) substrates as electrodes. Vertically aligned CNTs provide a large surface area, highly porous substrate with mechanical flexibility to relieve stresses in the active material. While carbon-based materials are widely used for supercapacitor applications, there is growing interest in developing silicon-based supercapacitor electrodes.[33–39] The advantages of Si as an electrode material include: opportunities for integration as micro-energy storage for on-chip devices such as sensors and actuators; high conductivity of doped Si; and the use of a low cost, highly abundant material.[33,34] The electrochemical instability of Si in aqueous electrolytes, however, is a challenge for Si-based pseudocapacitors fabricated by conventional, solution-based methods.[34,35] The ALD RuO_x-porous Si supercapacitors in this work demonstrate an effective means to achieve high performance Si-based micro-supercapacitors.

Experimental

CNT and Porous Si - based ALD RuO_x electrodes

Vertically aligned CNTs were synthesized on silicon substrates by chemical vapor deposition using iron and aluminum catalyst layers, as described by Jiang et al[5] and illustrated schematically in Supplementary Information Figure S1. The substrates were first cleaned in pirahna solution (heated mixture of sulfuric acid and hydrogen peroxide), then coated with 100 μm thermally grown silicon dioxide as a barrier against metal diffusion into the silicon. A 50 nm molybdenum electrical contact layer was deposited by electron-beam evaporation, followed by the metal catalyst layers (10 nm aluminum and 5 nm iron by thermal evaporation). CNTs were grown in a horizontal tube furnace at 720 ºC and atmospheric pressure in a mixture of 7:1 hydrogen-to-ethylene gas. A growth time of 10 minutes gave CNT heights of approximately 10 μm. Porous Si electrodes were synthesized by HF anodization using a p-type Si substrate. The substrate was placed between two electrodes in an aqueous HF-ethanol solution (10% hydrofluoric acid, 20% ethanol) in a Teflon container. A current of 6 – 12 mA/cm^2 was applied between both sides of the substrate according to the constant current anodization method.[40,41]

RuO_x was deposited using a Cambridge Fiji F200 Plasma ALD with bis(ethylcyclopentadienyl)ruthenium(II) ($Ru(EtCp)_2$) and oxygen (O_2) as precursors. Pulse times for $Ru(EtCp)_2$ and O_2 were 1 s and 10 s respectively, with 5 s argon gas purge times. During the ALD process, substrates were heated to temperatures ranging from 270 ºC to 400 ºC. Electrochemical oxidation of ALD RuO_x electrodes was conducted in 0.5 M H_2SO_4 electrolyte by controlled potential coulometry at 1.3 V vs. Ag/AgCl reference electrode for times ranging from 3 min to 120 min. Thermal oxidation of ALD RuO_x supercapacitor electrodes was conducted in a horizontal tube furnace at 600 ºC for 30 min with 70 sccm O_2 flow.

Electrochemistry

Electrochemical testing was conducted in 0.5 M H_2SO_4 electrolyte using a Gamry Reference 600 potentiostat. Cyclic voltammetry (CV) measurements were performed using a three-electrode test set-up with a platinum counter electrode and Ag/AgCl reference electrode. All samples were cycled for at least 20 CV cycles to stabilize prior to performance testing. A scan rate of 100 mV/s was used for CV measurements, unless otherwise indicated. Constant current charge-discharge (chronopotentiometry)

Journal of Materials Chemistry A Accepted Manuscript

measurements were performed using a symmetrical, two-electrode test cell without separator. For ALD RuO_x-CNT electrodes, the mass of active material is approximately 1.3 mg/cm^2 of electrode planar surface area, as calculated from RuO_x thickness measurements and measured CNT densities (1.4 mg/cm^2 for electrochemically oxidized ALD RuO_x-CNT electrodes, taking into account the increase in mass of the ALD coating with oxidation). The estimated active material mass for porous Si electrodes is 20.4 mg/cm^2. Further details of active mass measurements are provided in the Supplementary Information.

Materials Characterization

Scanning electron microscopy (SEM) images were taken using an FEI Nova NanoSEM 650 scanning electron microscope and transmission electron microscopy (TEM) images with a Technai 12 transmission electron microscope. X-ray diffraction (XRD) measurements were conducted with a Siemens D5000 X-Ray Diffractometer (Cu Kα radiation) and X-ray photoelectron spectroscopy (XPS) measurements with a PHI Quantum 2000 X-ray photoelectron spectrometer.

Results and Discussion

Figure 1a provides a conceptual illustration of ALD RuO_x in uniformly coated porous supercapacitor electrodes. A generic porous structure is coated with ALD RuO_x by sequential pulsing of gas-phase precursors of $Ru(EtCp)_2$ and oxygen. A scanning electron microscope (SEM) image of vertically aligned CNTs coated with ALD RuO_x shows uniform coating over the entire length of the CNTs (Figure 1b). TEM images indicate that the as-deposited films are polycrystalline and highly conformal (Figure 1c and Figure S2). SEM images of ALD RuO_x films deposited on porous Si electrodes are provided in the Supplementary Information (Figure S3). For porous Si electrodes, RuO_x is deposited over the entire depth of the pores (exceeding 127 μm) but with less uniformity than on CNTs due to poorer nucleation of ALD RuO_x on Si-H terminated surfaces.[42]

XPS measurement of ALD RuO_x deposited on planar substrates reveals significant oxide content in the surface region of the ALD films. XPS measurements of the Ru3d peak show a shift to higher binding energies – hence higher oxidation states – compared to Ru metal (Figure 1d). Since ruthenium does not form a native oxide at room temperature,[43] these results suggest that the observed RuO_2 surface layer is formed during the ALD process. XRD measurements of as-deposited ALD RuO_x on a planar substrate (Figure S4) indicate a metallic ruthenium crystal structure (Ru(100)), suggesting that the films are not fully oxidized. During the ALD process, the oxygen precursor both oxidatively decomposes the organometallic ruthenium precursor and oxidizes the depositing Ru metal; *in-situ* ALD RuO_x formation can therefore be inhibited by low rates of subsurface oxygen absorption[44] and slow reaction kinetics for Ru oxidation.[30] XRD and XPS measurements for CNT electrodes are similar to planar electrodes, and are provided in the Supplementary Information (Figures S5, S6).

Journal of Materials Chemistry A Accepted Manuscript

Journal of Materials Chemistry A Accepted Manuscript

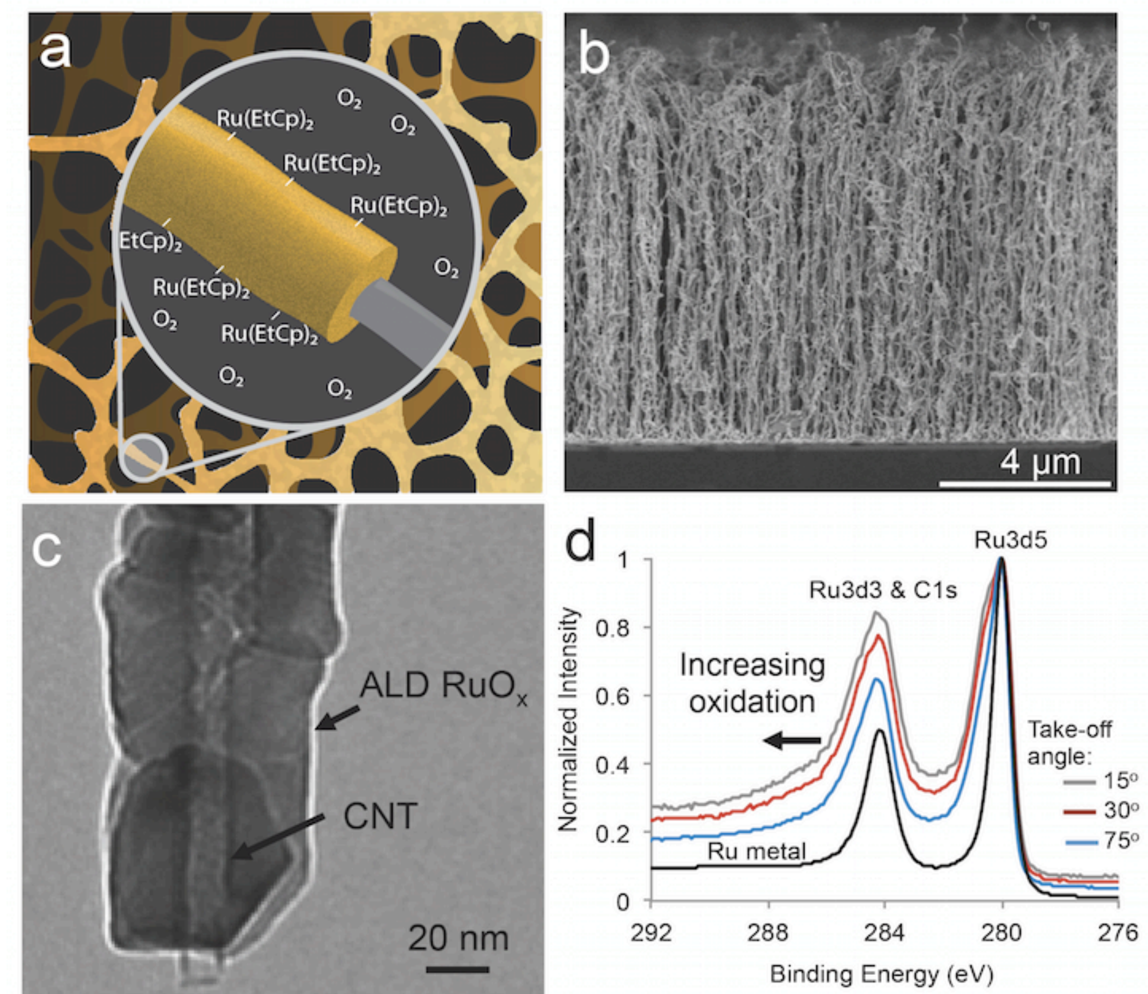

Figure 1. Conceptual illustration and demonstration of ALD RuO_x supercapacitor electrodes. (a) Schematic drawing of RuO_x deposited uniformly and conformally on a high surface area, porous electrode by ALD. Monolayer by monolayer deposition is achieved by sequential pulsing of $Ru(EtCp)_2$ and oxygen. (b) SEM image of vertically aligned CNTs coated with ALD RuO_x. (c) TEM image of a single CNT conformally coated with ALD RuO_x. (d) High-resolution XPS measurements of Ru3d binding energy for as-deposited ALD RuO_x films on planar electrodes. The Ru3d peak shows a shift to higher binding energies, hence higher oxidation state, compared to Ru metal.

Cyclic voltammetry (CV) measurements were conducted to determine the specific capacitance of ALD RuO_x supercapacitor electrodes (capacitance calculations and electrode mass measurements are provided in the Supplementary Information). Specific capacitance is an important performance metric because it corresponds to the energy storage of pseudocapacitors ($E = ½ CV^2$). Figure 2a provides a comparison of the CV curves for ALD RuO_x-CNT electrodes deposited at ALD temperatures of 270 ºC – 400 ºC. The as-deposited ALD RuO_x films are highly capacitive, and the shape of the CV curves is characteristic of RuO_2 supercapacitors.[20,45] Although the ALD RuO_x coatings are

not fully oxidized, there is a large, two-order of magnitude increase in specific capacitance for vertically aligned CNT electrodes with the ALD RuO_x coating, from 3.4 F/g (0.47 mF/cm^2) for uncoated CNTs (Figure S14a) to a maximum of 363 F/g for ALD RuO_x-CNTs (404 F/g counting only the mass of RuO_x) (23.6 mF/cm^2). We observe that the pseudocapacitive performance is highly dependent on the ALD temperature, with lower deposition temperatures corresponding to higher CV currents. Lowering the ALD temperature from 400 ºC to 270 ºC results in a 4.4x enhancement in ALD RuO_x-CNT specific capacitance (2.4x enhancement from 400 ºC to 350 ºC) (Figure 2a). This result is indicative of the degree of hydration of the ALD films, as metal oxide pseudocapacitance is highly dependent on hydration state and proton conductivity of the oxide.[16,21] Studies have found that RuO_2 dehydration begins at temperatures above 150 ºC, with increasing temperatures accelerating water loss until full dehydration occurs at 400 ºC.[45,46] The temperature dependence of capacitance shown in Figure 2a is particularly interesting because it suggests that ALD metal oxide films, in particular hygroscopic oxides like RuO_x,[47] can be deposited in a hydrated state. High resolution XPS measurements of ALD RuO_x films deposited at 350 ºC support this hypothesis, with XPS curve fitting of the O 1s peak (Figure S15) closely matching that reported by Mun *et al*. for hydrous RuO_2, and differing substantially from anhydrous RuO_2 curves presented in Mun *et al*.[48] This important result, observed for ALD RuO_x supercapacitors, is significant for ALD metal oxide pseudocapacitors in general, as ALD reactions typically occur in the temperature range of metal oxide dehydration (Table 1).

Life cycle testing of ALD RuO_x supercapacitor electrodes was conducted by repeated CV scans over the full supercapacitor operating range (0 – 1.0 V) (Figure 2b). Remarkably, the specific capacitance of the ALD RuO_x-CNT electrode increases by 17% after 10,000 CV cycles. We observe a change in the shape of the CV curves from cycle 10 to cycle 10,000 with evidence of a RuO_x peak,[20,45] suggesting a non-reversible change in the electrode material chemistry. We believe this performance improvement is due to the gradual electrochemical oxidation of as-deposited ALD RuO_x during the CV cycles.[49,50] A similar increase in capacitance was observed with repeated cycling of planar ALD RuO_x (Figure S16), however the durability of the planar electrode is much lower than that of CNTs. After 3000 cycles, we observed significant damage to the planar ALD RuO_x electrode, likely due to stresses in the RuO_x film from repeated cycling between redox states on an inflexible substrate. The surprising results of lifecycle testing of ALD RuO_x-CNT electrodes suggest that post-ALD electrochemical oxidation could be used to achieve highly active RuO_x and a further increase in specific capacitance by converting the mixed metal-oxide ALD films to hydrated amorphous RuO_x. In the following, we explore this theory by testing the performance of post-ALD electrochemically oxidized supercapacitor electrodes, with an aim to achieve ultra-high charge storage capability.

Journal of Materials Chemistry A Accepted Manuscript

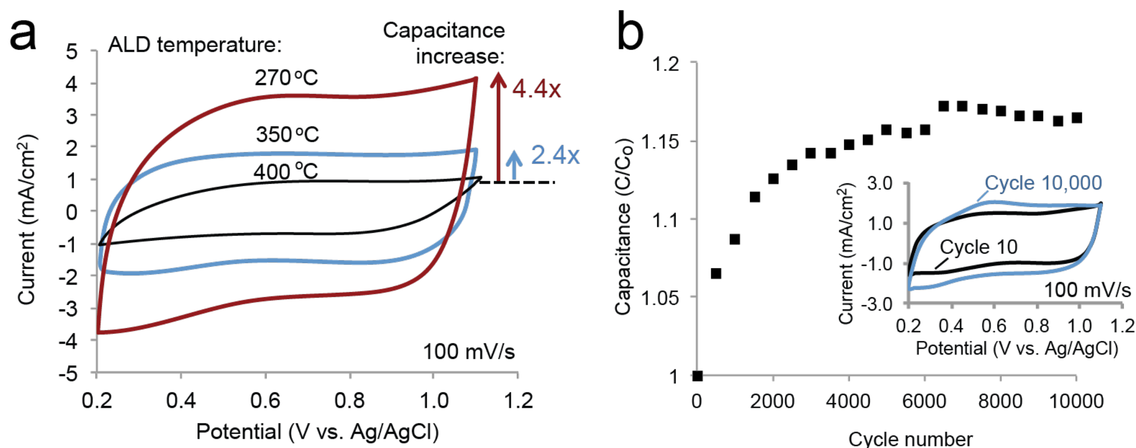

Figure 2. Performance testing of ALD RuO_x-CNT supercapacitor electrodes. (a) CV measurements of ALD RuO_x-CNT electrodes deposited at 270 °C – 400 °C, demonstrating enhanced pseudocapacitance at lower ALD temperatures (capacitance increases of 2.4x and 4.4x for 350 °C and 270°C, respectively, compared to 400 °C deposition temperature). (b) Life cycle testing of ALD RuO_x-CNT electrodes shows a 17% increase in specific capacitance after 10,000 CV cycles. Inset: Change in shape of CV curves after 10 vs. 10,000 cycles, indicating non-reversible electrochemical oxidation of the RuO_x-CNT electrode.

Table 1: Comparison of dehydration temperatures and typical ALD deposition temperatures for select pseudocapacitive metal oxides.

Metal oxide	Dehydration temperature		Typical ALD temperature
	50% dehydrated	Fully dehydrated	
Ruthenium oxide	130 °C[45]	400 °C[45]	270– 400 °C[32,51]
Vanadium oxide	90 °C[52]	350 °C[52]	50 – 200 °C[53]
Manganese oxide	190 °C[54]	400 °C[54]	140 – 210 °C[55,56]
Cobalt oxide	160 °C[57]	170 °C[57]	190 – 280 °C[58]

Figure 3a, following from Figure 1a, illustrates the use of post-ALD electrochemical oxidation to improve proton conductivity and enhance charge storage in the pseudocapacitive metal oxide (details of the electrochemical oxidation process are provided in the Experimental section). Thermal oxidation was used as a comparison to determine the relative impact of increased oxidation vs. hydration of the ALD films. SEM images of vertically aligned CNT electrodes indicate there is no degradation of the ALD coating or CNT structure with electrochemical or thermal oxidation (Figure S17). TEM images show a 29% increase in RuO_x thickness with thermal oxidation, and a 35% increase with 9 minutes of electrochemical oxidation (Table S3). XRD measurements of

Journal of Materials Chemistry A Accepted Manuscript

thermally and electrochemically oxidized ALD RuO_x show RuO_2(210) and mixed RuO_2(110)/RuO_2(101) peaks, respectively (Figure S18). XRD measurements indicate that the electrochemically-oxidized film has greater amorphous character, likely due to its hydrated structure with incorporated water molecules distorting the polycrystalline structure.[46]

Comparing CV measurements for as-deposited and electrochemically oxidized ALD RuO_x- CNT and porous Si electrodes, there is a substantial increase in supercapacitor charging and discharging currents with post-ALD electrochemical oxidation (Figure 3b,c) . Specifically, the electrochemically oxidized ALD RuO_x-CNT electrode reaches a maximum capacitance value of 644 F/g (counting only the mass of RuO_x; 578 F/g including the mass of CNTs) (37.7 mF/cm^2), an increase of 170x that of uncoated CNTs and in the same order of magnitude as the theoretical capacitance of RuO_2 at 1450 F/g.[59] For porous Si electrodes, specific capacitance increases from an uncoated value of 0.39 mF/g (15.4 μF/cm^2) (Figure S14b) to 1.88 F/g (38.2 mF/cm^2) with as-deposited ALD RuO_x to 2.42 F/g (49.2 mF/cm^2) with electrochemically oxidized ALD RuO_x – a 6200x increase and the highest value of gravimetric specific capacitance reported for porous Si-based electrodes.[33,60] In contrast, thermal oxidation of ALD RuO_x electrodes results in a decrease in specific capacitance by 55% for CNT electrodes when compared to as-deposited ALD RuO_x. This observed loss in supercapacitor performance is most likely due to dehydration of the ALD RuO_x with thermal oxidation, despite the increase in oxide content of the ALD film. Figure 3d shows the effect of increasing electrochemical oxidation time on the specific capacitance of ALD RuO_x-CNT and RuO_x-porous Si (inset) supercapacitor electrodes. The capacitance of ALD RuO_x-CNT electrodes increases steadily over 120 minutes of electrochemical oxidation. For porous Si electrodes, however, we observe a decrease in capacitance after 3 minutes of oxidation, and a substantial degradation of both the ALD RuO_x film and porous Si substrate after 18 minutes of electrochemical oxidation (Figure S19). We attribute these results to differences in each electrode's ability to accommodate stresses in the ALD RuO_x film arising from simultaneous oxidation and hydration processes, with the vertically aligned CNT forest providing a highly flexible electrode substrate.[61]

Journal of Materials Chemistry A Accepted Manuscript

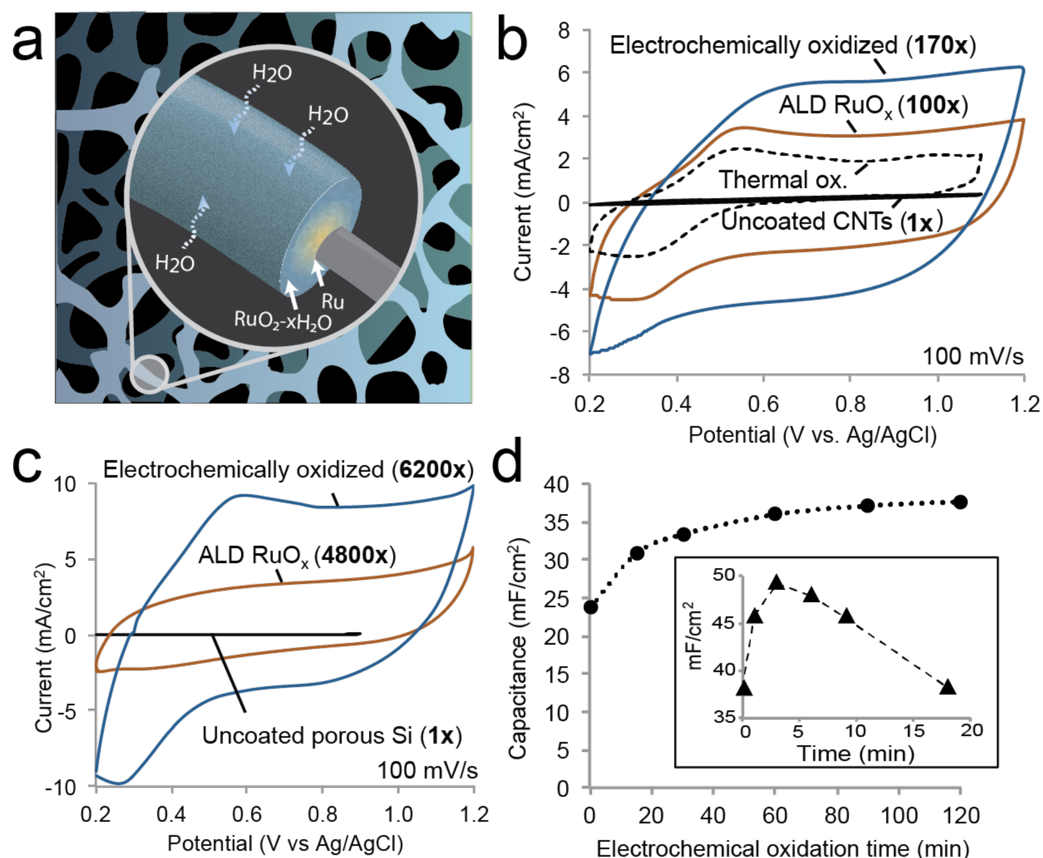

Figure 3. Conceptual illustration and demonstration of enhanced pseudocapacitance with post-ALD electrochemical oxidation. (a) Chemical activation to create a hydrated RuO_x supercapacitor electrode with high proton conductivity. (b), (c), CV measurements of CNT and porous Si ALD RuO_x electrodes, respectively. Electrochemical oxidation improves capacitance, while thermal oxidation ("Thermal ox.") decreases capacitance compared to as-deposited ("ALD RuO_x") electrodes. CV measurements for uncoated CNT and uncoated porous Si electrodes are included for comparison (for full details, see Figure S14). (d) Change in capacitance of ALD RuO_x-CNT electrodes with electrochemical oxidation time, with a continuous increase in specific capacitance over 120 minutes of oxidation. Inset: Capacitance of ALD RuO_x-porous Si increases for 3 minutes of electrochemical oxidation, then decreases as a result of damage to the porous Si electrode.

Constant current charge-discharge (chronopotentiometry) measurements of symmetric, two-electrode test cells are used to determine power and energy density of the ALD RuO_x supercapacitors (Figure 4a and S20). Charge-discharge curves for planar ALD RuO_x electrodes show good linearity with low resistance drop for both as-deposited and electrochemically oxidized ALD films, indicating fast and highly reversible redox reactions. Figure 4b provides a Ragone plot of power and energy density for planar and CNT-based ALD RuO_x supercapacitor electrodes (power and energy density calculations are included in the Supplementary Information). Electrochemical oxidation of as-

Journal of Materials Chemistry A Accepted Manuscript

deposited ALD films results in a substantial improvement in energy and power density for planar RuO_x electrodes (17x increase in maximum power density and 14x increase in maximum energy density). The highest power density achieved for the ALD supercapacitor electrodes is 17 kW/kg for electrochemically oxidized planar RuO_x. For CNT electrodes, energy density is also highest with the electrochemically oxidized ALD RuO_x coating at 4.0 Wh/kg. Power density, in contrast, is greatest for uncoated CNT electrodes as a result of the faster charge/discharge mechanism for double layer capacitance compared to pseudocapacitance. Electrochemical oxidation further decreases the power density of ALD RuO_x-CNT electrodes, likely due to an increase in pseudocapacitance vs. double layer capacitance as the primary energy storage mechanism of the electrochemically oxidized CNT electrodes. In general, energy and power density of the CNT-based electrodes are lower than expected, and charge-discharge curves for ALD RuO_x-CNT electrodes show greater non-linearity and higher resistance drop compared to planar electrodes (Figure S20c, d). Similar non-linearities are observed for uncoated CNTs (Figure S20e), suggesting side reactions arising from impurities present in the CNT electrodes rather than the ALD RuO_x coating. The relatively large IR drop observed for uncoated CNTs could be due to high resistance at the CNT-Mo contact.

CV scan rate tests have been conducted to characterize supercapacitor performances at different charging speeds (Figure 4c, d). Planar, as-deposited ALD RuO_x electrodes exhibit exceptional capacitance retention at high scan rates, maintaining the same specific capacitance at 10 mV/s and 20 V/s – one of the fastest scan rates reported (Figure S21). Electrochemical oxidation of as-deposited ALD RuO_x films generally improves capacitance retention at high scan rates. As shown in Figure 4d, increasing the oxidation time of ALD RuO_x-CNT electrodes from 18 min to 120 min enables the supercapacitors to maintain an additional 22% of their 10 mV/s specific capacitance value at a scan rate of 500 mV/s. We attribute this enhanced performance at higher scan rates to improved proton conductivity and hence faster redox reactions in the electrochemically oxidized ALD RuO_x films. Life cycle testing of electrochemically oxidized ALD RuO_x-CNTs tested over repeated charge-discharge cycles show a 19% decrease in specific capacitance after 1500 cycles (Figure S22), possibly the result of irreversible side-reactions arising from impurities in the CNT electrodes.

Journal of Materials Chemistry A Accepted Manuscript

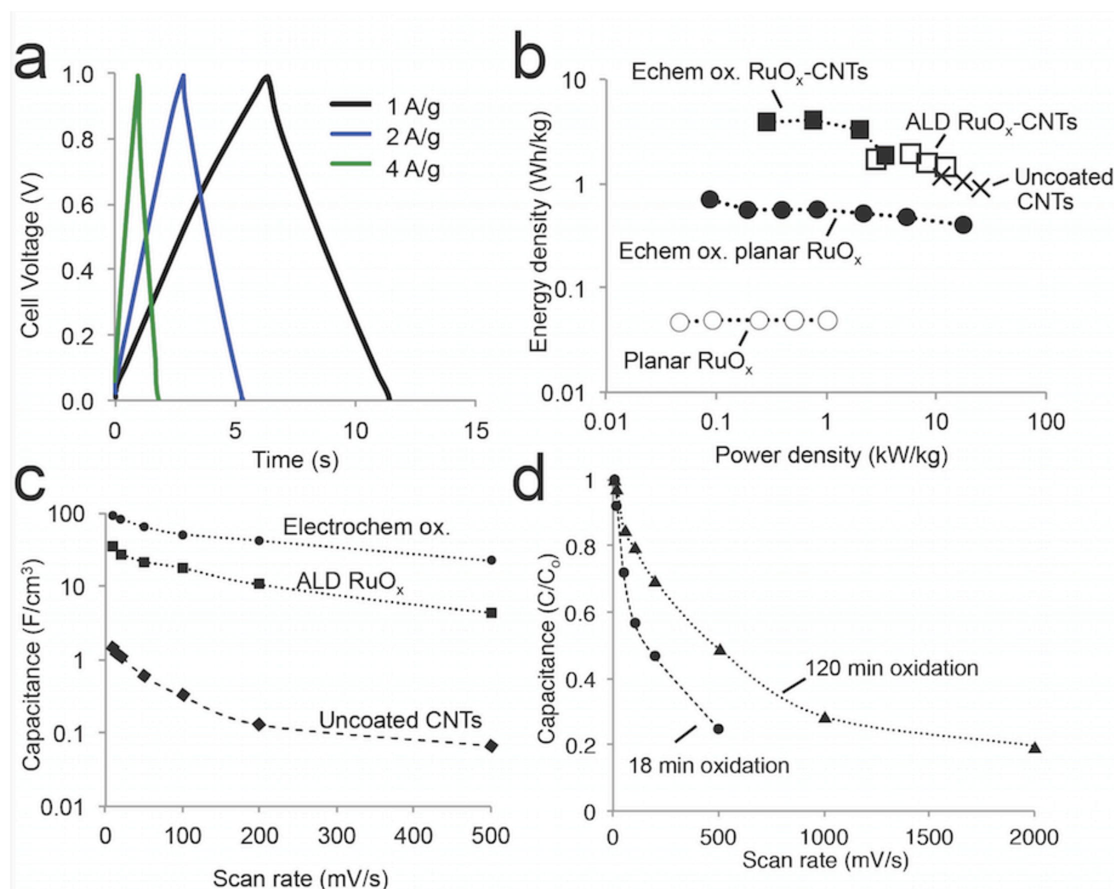

Figure 4. Power and energy density, as well as high scan rate performance testing of ALD RuO_x supercapacitor electrodes. (a) Constant current charge-discharge measurements of electrochemically oxidized planar ALD RuO_x (9 min oxidation time) show excellent linearity and low resistance drop. (b) Ragone plot comparing power and energy densities of planar and CNT-based ALD RuO_x supercapacitor electrodes (as-deposited and electrochemically oxidized), as well as uncoated CNTs. (c) Capacitance of uncoated CNT, as-deposited ALD RuO_x-CNT, and electrochemically oxidized ALD RuO_x-CNT electrodes at scan rates of 10 mV/s to 500 mV/s. (d) Increased capacitance retention of ALD RuO_x-CNT electrodes at high scan rates with increasing electrochemical oxidation time (18 min and 120 min electrochemical oxidation times compared).

Conclusions

In conclusion, we demonstrate the use of ALD to fabricate high-performance RuO_x supercapacitors, achieving conformal coating of high surface area electrodes and nanoscale control of film thickness. The as-deposited ALD RuO_x electrodes are mixed Ru/RuO_2, with some hydration at lower ALD reaction temperatures. Post-ALD electrochemical oxidation improves the specific capacitance, power density, energy density, and high scan rate performance of the ALD RuO_x supercapacitor electrodes by creating a hydrated, amorphous oxide with enhanced proton conductivity. The pseudocapacitive properties of the ALD RuO_x films include: excellent linearity; fast, reversible redox reactions; and exceptional life cycle performance. Results of this study are generally applicable to other pseudocapacitive metal oxides - such as manganese oxide, vanadium oxide, and mixed cobalt-nickel oxides - in which charge storage efficiency depends on achieving highly uniform, conformal electrode coatings with enhanced proton conductivity.

Journal of Materials Chemistry A Accepted Manuscript

Corresponding Author

* Liwei Lin, lwlin@berkeley.edu

Acknowledgements

The authors would like to thank: J. Chukes and R. Rivers from the UC Berkeley Marvell Nanofabrication Laboratory for their assistance with the ALD process; J. Clarkson from the Marvell Nanofabrication Laboratory for assistance with porous Si SEM imaging; M. Neuburger and D. Susnitzky from Evans Analytical Group for assistance with XPS measurements and high-resolution TEM imaging; and B. Hsia, A. Kozinda, and M. Stoller for helpful discussions of supercapacitor measurement techniques.

References

1. G. Wang, L. Zhang and J. Zhang, *Chem. Soc. Rev.*, 2012, **41**, 797–828.
2. M. Zhi, C. Xiang, J. Li, M. Li and N. Wu, *Nanoscale*, 2013, **5**, 72–88.
3. A. Yu, *Electrochemical supercapacitors for energy storage and delivery: fundamentals and applications*, CRC Press, Boca Raton, FL, USA, 2013.
4. R. Warren, F. Sammoura, K. S. Teh, A. Kozinda, X. Zang and L. Lin, *Sensors Actuators A Phys.*, 2014.
5. Y. Jiang, P. Wang, X. Zang, Y. Yang, A. Kozinda and L. Lin, *Nano Lett.*, 2013, **13**, 3524–3530.
6. P. Simon and Y. Gogotsi, *Nat. Mater.*, 2008, **7**, 845–54.
7. W. Wang, S. Guo, I. Lee, K. Ahmed, J. Zhong, Z. Favors, F. Zaera, M. Ozkan and C. S. Ozkan, *Sci. Rep.*, 2014, **4**, 4452–4460.
8. M. Ghaemi, F. Ataherian, a. Zolfaghari and S. M. Jafari, *Electrochim. Acta*, 2008, **53**, 4607–4614.
9. Z. Fan, J. Yan, T. Wei, L. Zhi, G. Ning, T. Li and F. Wei, *Adv. Funct. Mater.*, 2011, **21**, 2366–2375.
10. X. Lang, A. Hirata, T. Fujita and M. Chen, *Nat. Nanotechnol.*, 2011, **6**, 232–236.
11. X. Zhang, P. Yu, H. Zhang, D. Zhang, X. Sun and Y. Ma, *Electrochim. Acta*, 2013, **89**, 523–529.
12. X. Zhang, X. Sun, H. Zhang, C. Li and Y. Ma, *Electrochim. Acta*, 2014, **132**, 315–322.
13. I.-H. Kim, J.-H. Kim, B.-W. Cho, Y.-H. Lee and K.-B. Kim, *J. Electrochem. Soc.*, 2006, **153**, A989–A996.
14. C.-C. Hu and C.-Y. Cheng, *Electrochem. Solid-State Lett.*, 2002, **5**, A43–A46.
15. J. P. Zheng, P. J. Cygan and T. R. Jow, *J. Electrochem. Soc.*, 1995, **142**, 2699–2703.
16. M. T. Brumbach, T. M. Alam, P. G. Kotula, B. B. McKenzie and B. C. Bunker, *ACS Appl. Mater. Interfaces*, 2010, **2**, 778–787.
17. R. Bi, X. Wu, F. Cao, L. Jiang, Y. Guo and L. Wan, *J. Phys. Chem. C*, 2010, **114**, 2448–2451.
18. T. F. Hsieh, C. C. Chuang, W. J. Chen, J. H. Huang, W. T. Chen and C. M. Shu, *Carbon*, 2012, **50**, 1740–1747.
19. J. Zhang, J. Jiang, H. Li and X. S. Zhao, *Energy Environ. Sci.*, 2011, **4**, 4009–4015.
20. C. C. Hu and C. C. Wang, *Electrochem. commun.*, 2002, **4**, 554–559.
21. V. D. Patake, C. D. Lokhande and O. S. Joo, *Appl. Surf. Sci.*, 2009, **255**, 4192–4196.

Journal of Materials Chemistry A Accepted Manuscript

22. J. K. Lee, H. M. Pathan, K. D. Jung and O. S. Joo, *J. Power Sources*, 2006, **159**, 1527–1531.
23. J. S. Ye, H. F. Cui, X. Liu, T. M. Lim, W. De Zhang and F. S. Sheu, *Small*, 2005, **1**, 560–565.
24. G. Cui, L. Zhi, A. Thomas, I. Lieberwirth, U. Kolb and K. Müllen, *ChemPhysChem*, 2007, **8**, 1013–1015.
25. C.-C. Hu, W.-C. Chen and K.-H. Chang, *J. Electrochem. Soc.*, 2004, **151**, A281–A290.
26. S. M. George, *Chem. Rev.*, 2010, **110**, 111–131.
27. C. Marichy, M. Bechelany and N. Pinna, *Adv. Mater.*, 2012, **24**, 1017–1032.
28. S. Boukhalfa, K. Evanoff and G. Yushin, *Energy Environ. Sci.*, 2012, **5**, 6872–6879.
29. X. Sun, M. Xie, G. Wang, H. Sun, A. S. Cavanagh, J. J. Travis, S. M. George and J. Lian, *J. Electrochem. Soc.*, 2012, **159**, A364–A369.
30. B. T. Aaltonen, P. Aløn, M. Ritala and M. Leskelä, *Chem. Vap. Depos.*, 2003, **9**, 45–49.
31. O.-K. Kwon, J.-H. Kim, H.-S. Park and S.-W. Kang, *J. Electrochem. Soc.*, 2004, **151**, G109.
32. W.-H. Kim, S.-J. Park, D. Y. Kim and H. Kim, *J. Korean Phys. Soc.*, 2009, **55**, 32–37.
33. L. Oakes, A. Westover, J. W. Mares, S. Chatterjee, W. R. Erwin, R. Bardhan, S. M. Weiss and C. L. Pint, *Sci. Rep.*, 2013, **3**, 3020–3026.
34. J. P. Alper, M. Vincent, C. Carraro and R. Maboudian, *Appl. Phys. Lett.*, 2012, **100**, 32–36.
35. J. P. Alper, M. S. Kim, M. Vincent, B. Hsia, V. Radmilovic, C. Carraro and R. Maboudian, *J. Power Sources*, 2013, **230**, 298–302.
36. M. Li, S. Xu, T. Liu, F. Wang, P. Yang, L. Wang and P. K. Chu, *J. Mater. Chem. A*, 2013, **1**, 532–540.
37. F. Miao, B. Tao, P. Ci, J. Shi, L. Wang and P. K. Chu, *Mater. Res. Bull.*, 2009, **44**, 1920–1925.
38. T. Liu, S. Xu, L. Wang, J. Chu, Q. Wang, X. Zhu, N. Bing and P. K. Chu, *J. Mater. Chem.*, 2011, **21**, 19093–19100.
39. F. Thissandier, N. Pauc, T. Brousse, P. Gentile and S. Sadki, *Nanoscale Res. Lett.*, 2013, **8**, 38–42.
40. A. G. Cullis, L. T. Canham and P. D. J. Calcott, *J. Appl. Phys.*, 1997, **82**, 909–965.
41. É. Vázsonyi, E. Szilágyi, P. Petrik, Z. E. Horváth, T. Lohner, M. Fried and G. Jalsovszky, *Thin Solid Films*, 2001, **388**, 295–302.
42. K. J. Park, K. J. Park, D. B. Terry, D. B. Terry, S. M. Stewart, S. M. Stewart, G. N. Parsons, G. N. Parsons, N. Carolina and N. Carolina, *Langmuir*, 2007, 6106–6112.
43. B. Herd, J. C. Goritzka and H. Over, *J. Phys. Chem. C*, 2013, **117**, 15148–15154.
44. R. Methaapanon, S. M. Geyer, S. Brennan and S. F. Bent, *Chem. Mater.*, 2013, **25**, 3458–3463.
45. J. P. Zheng and T. R. Jow, *J. Electrochem. Soc.*, 1995, **142**, L6–L8.
46. D. A. Mckeown, P. L. Hagans, L. P. L. Carette, A. E. Russell, K. E. Swider and D. R. Rolison, *J. Phys. Chem. B*, 1999, **103**, 4825–4832.
47. H. Y. H. Chan, C. G. Takoudis and M. J. Weaver, *J. Catal.*, 1997, **172**, 336–345.
48. C. Mun, J. J. Ehrhardt, J. Lambert and C. Madic, *Appl. Surf. Sci.*, 2007, **253**, 7613–7621.
49. S. Hadz̄i-Jordanov, H. Angerstein-Kozlowska, M. Vukovic and B. E. Conway, *J. Electrochem. Soc.*, 1978, **125**, 1471–1480.
50. L. D. Burke, J. K. Mulcahy and S. Venkatesan, *J. Electroanal. Chem.*, 1977, **81**, 339–346.

Journal of Materials Chemistry A Accepted Manuscript

51. S. Park, W. Kim, W. Maeng and Y. Yang, *Thin Solid Films*, 2008, **516**, 7345–7349.
52. F. Chaput, B. Dunn, P. Fuqua and K. Salloux, *J. Non. Cryst. Solids*, 1995, **188**, 11–18.
53. J. Badot, S. Ribes, E. Yousfi, V. Vivier, J. P. Pereira-Ramos, N. Baffier and D. Lincot, *Electrochem. Solid-State Lett.*, 2000, **3**, 485–488.
54. E. Raymundo-Pinero, V. Khomenko, E. Frackowiak and F. Beguin, *J. Electrochem. Soc.*, 2005, **152**, A229–A235.
55. O. Nilsen, H. Fjellvåg and A. Kjekshus, *Thin Solid Films*, 2003, **444**, 44–51.
56. N. C. Strandwitz, D. J. Comstock, R. L. Grimm, A. C. Nichols-Nielander, J. Elam and N. S. Lewis, *J. Phys. Chem. C*, 2013, **117**, 4931–4936.
57. C. Lin, J. Ritter and B. Popov, *J. Electrochem. Soc.*, 1998, **145**, 4097–4103.
58. K. B. Klepper, O. Nilsen and H. Fjellvåg, *J. Cryst. Growth*, 2007, **307**, 457–465.
59. M. Min, K. Machida, J. H. Jang and K. Naoi, *J. Electrochem. Soc.*, 2006, **153**, A334–A338.
60. S. E. Rowlands, R. J. Latham and W. S. Schlindwein, *Ionics*, 1999, **5**, 144–149.
61. S. Iijima, C. Brabec, A. Maiti and J. Bernholc, *J. Chem. Phys.*, 1996, **104**, 2089–2092.

Journal of Materials Chemistry A Accepted Manuscript

Graphical Abstract

Highly active ruthenium oxide coating via ALD and electrochemical activation in supercapacitor applications

Roseanne Warren, Firas Sammoura, Fares Tounsi, Mohan Sanghadasa and Liwei Lin

Vertically aligned CNTs exhibit 100x and 170x higher capacitance when coated with ALD RuO_x and after further electrochemical oxidation, respectively.

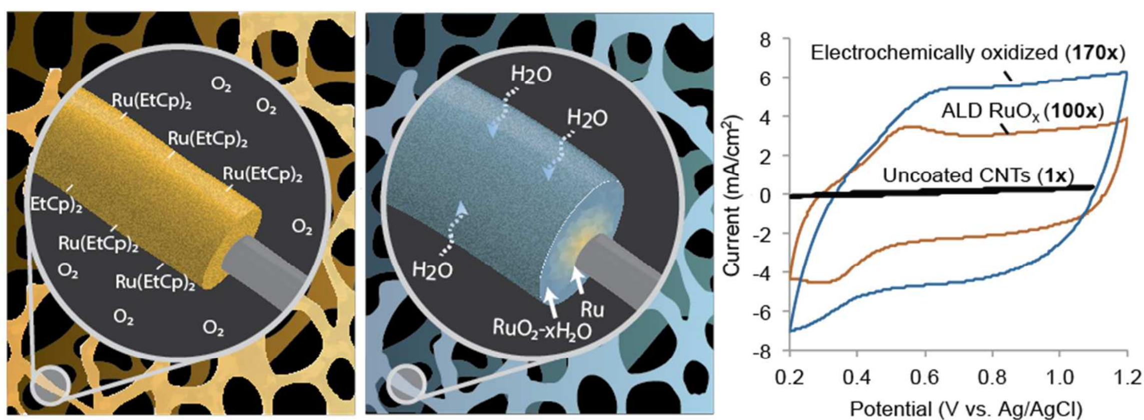

Journal of Materials Chemistry A Accepted Manuscript